Journal of Alloys and Compounds 590 (2014) 346–354

Contents lists available at ScienceDirect

Journal of Alloys and Compounds

journal homepage: www.elsevier.com/locate/jalcom

Effects of Mn doping on multiferroic and magnetocapacitive properties of $0.33Ba_{0.70}Ca_{0.30}TiO_3$–$0.67BiFeO_3$ diphasic ceramics

Cai-Xia Li [a,b], Bin Yang [a,*], Shan-Tao Zhang [c,*], Dan-Qing Liu [d], Rui Zhang [a], Ye Sun [a], Wen-Wu Cao [a,e]

[a] Department of Physics, Condensed Matter Science and Technology Institute, Harbin Institute of Technology, Harbin 150001, China
[b] Department of Material Physics, School of Applied Sciences, Harbin University of Science and Technology, Harbin 150080, China
[c] Department of Materials Science and Engineering & National Laboratory of Solid State Microstructures, Nanjing University, Nanjing 210093, China
[d] School of Chemical Engineering and Technology, Harbin Institute of Technology, Harbin 150080, China
[e] Materials Research Institute, The Pennsylvania State University, University Park, PA 16802, USA

ARTICLE INFO

Article history:
Received 3 August 2013
Received in revised form 5 November 2013
Accepted 6 November 2013
Available online 16 November 2013

Keywords:
$0.33Ba_{0.70}Ca_{0.30}TiO_3$–$0.67BiFeO_3$ ceramics
Mn doping
Magnetocapacitive effect
Multiferroic properties

ABSTRACT

The $0.33Ba_{0.70}Ca_{0.30}TiO_3$–$0.67BiFeO_3$ + x wt% MnO_2 (BCT-67BF:Mn100x, x = 0–0.6) multiferroic ceramics have been prepared. The effects of Mn doping on structures, electric, magnetic as well as magnetocapacitive properties have been intensively investigated. It is found that all the ceramics have diphasic tetragonal-rhombohedral phases, whereas Mn doping improves the densification and significantly decreases the grain size. As x increases, the relaxor degree increases, the ferroelectricity and piezoelectricity weaken monotonically, while the magnetism enhances firstly, reaching the maximum near x = 0.5, and then decreases. Interestingly, the room temperature relative dielectric constant shows an obvious increase with increasing applied magnetic fields (H), the magnetocapacitive coefficient $(\varepsilon_r(H)-\varepsilon_r(0))/\ \varepsilon_r(0)$ decreases with increasing Mn content, from 2.96% for x = 0 – 0.86% for x = 0.6.

1. Introduction

Multiferroic materials exhibit a coexistence of different types of ferroic orders such as (anti)ferromagnetism, (anti)ferroelectricity and (anti)ferroelasticity. They have attracted a great deal of interests for their fascinating fundamental physics as well as the promising applications in multifunctional devices like data storage media, spinotronics, and sensors and actuator devices, [1–4]. The interactions between magnetic and electric polarizations in multiferroics can produce a number of additional functionalities, such as magnetocapacitive effect, in which the magnetization can be manipulated by the applied electric fields and *vice versa* [5–7]. Unfortunately, most of the reported single phase multiferroics exhibit rather weak ferromagnetism or antiferromagnetism without spontaneous magnetization, where the corresponding magnetocapacitive effect is almost negligible [8,9], in other words, the coexistence of ferroelectric (FE) and ferromagnetic (FM) orders in single phase material is rare [10]. This is reasonable because ferroelectric and magnetic orders may be mutually exclusive: It has been shown that ferroelectricity in ABO_3 perovskites generally originates from the off-center displacement of B-site transition metal cations (such as Ti^{4+} in $BaTiO_3$), which requires empty d orbitals for the hybridization of 3d Ti and 2p O orbitals [10–12]. However, magnetism requires transition metal ions with partially filled d orbitals and the breaking of the time reversal symmetry [6,10,11].

$BiFeO_3$ (BF) is one of the very few single phase multiferroics at room temperature (RT), one of the most widely studied and controversial multiferroic systems in recent years [11,13]. The Bi ion with 6 s^2 lone pair electrons can move away from the centrosymmetric position in its oxygen surroundings so lead to ferroelectricity [8,11,13], while the magnetism originates from the partially filled d orbitals of Fe [10,11]. BF has a rhombohedral distorted perovskite structure in the space group R3c at RT with a high FE Curie temperature (T_C) of 830 °C [6], and an antiferromagnetic Néel temperature (T_N) of 370 °C [14]. However, there are several drawbacks which hamper its practical technological applications [14,15]. The spatially modulated spin structure results in the weak magnetization at room temperature and inhibits the observation of linear magnetoelectric effect in the bulk BF. It is difficult to fabricate a single-phase BF material. The various impurity phases such as $Bi_2Fe_4O_9$, $Bi_{36}Fe_{24}O_{57}$, $Bi_{25}FeO_{40}$ result in high leakage current, making it difficult to obtain intrinsic ferroelectricity [15,16].

To resolve the above problems, many studies have endeavored to enhance the electric insulation resistance, ferroelectricity, magnetism and magnetocapacitive effect in BF-based multiferroic compounds. For example, making chemical substitutions [11,13,14], changing the manufacturing method [16], forming solid

* Corresponding authors.
E-mail addresses: binyang@hit.edu.cn (B. Yang), stzhang@nju.edu.cn (S.-T. Zhang).

0925-8388/$ - see front matter © 2013 Elsevier B.V. All rights reserved.
http://dx.doi.org/10.1016/j.jallcom.2013.11.029

solutions of BF and other ABO_3 ferroelectrics [1,17–19], etc. Generally, forming solid solutions or substituting for A/B-sites is the largely adopted way to increase the resistivity, enhance ferroelectric/magnetic properties and magnetocapacitive effect. For example, Xu et al. reported that the enhanced dielectric properties, frequency independence, and ferroelectric properties of Y and Zr co-doped BF ceramics were ascribed to the collapse of cycloidal spin structure induced by co-doping [20]. Yang et al. prepared single phase multiferroic ceramics of $(1-x)BaTiO_3-xBiFeO_3$ (BT-BF) solid solutions by solid state reaction method and observed the room temperature magnetoelectric coupling in the ceramics with $x = 0.71–0.80$ [8]. Kumar et al. also observed that the substitution of $BaTiO_3$ into $BiFeO_3$ enhanced dielectric, ferromagnetic responses and reduces electrical leakage [1]. Kubota et al. observed the weak ferromagnetism in Co doped BF ceramics and reported that the enhanced magnetism was ascribed to the change in the spin structure from a cycloidal one by Co doping [21]. And particularly, it is noted a small amount of aliovalent Mn doping can not only increase the resistivity, dielectric and piezoelectric properties [22–24], but also significantly improve its magnetic properties [14,22,25]. Wei et al. investigated the magnetic properties of hexagonal $Ba(Ti_{1-x}Mn_x)O_3$ ($x = 1/9$, $1/6$) ceramics specifically treated under different thermal conditions, they observed enhanced weak ferromagnetism with increasing Mn content in post-annealed ceramics [23].

On the other hand, it is noted diphasic materials generally can have superior properties than single phase counterparts. For instance, the high piezoelectric performance ($d_{33} \sim 568$pC/N) in $(Ba_{0.95}Ca_{0.05})(Ti_{0.92}Sn_{0.08})O_3$ ceramics is believed to result from the coupling between the two different equivalent energy states of the tetragonal (T) and orthorhombic (O) phases [26]. In addition, the ferroelectric and piezoelectric properties of diphasic $(Ba_{1-x}Ca_x)TiO_3$ (BCTx) ceramics near the solubility limit ($x = 0.23$) are much higher than that of the pure T phase BCTx ($x < 0.23$) and the pure R phase BCTx ($x > 0.90$), which are ascribed to the interaction between the large ionic polarization in O phase and the domains in T phase [27].

So, to improve sintering ability, enhance the electric resistivity, obtain good ferroelectric/magnetic multiferroic properties, and magnetocapacitive effect of BF-based materials, Mn doped $0.33Ba_{0.70}Ca_{0.30}TiO_3–0.67BiFeO_3$ solid solution was designed based on the above descriptions, and it is expected that the doping of aliovalent Mn ion may be helpful for improving FM and magnetocapacitive properties of the solid solutions [14,22]. In this paper, the structure, dielectric relaxor behavior, ferroelectric, piezoelectric, magnetic and magnetocapacitive properties of diphasic $0.33Ba_{0.70}Ca_{0.30}TiO_3–0.67BiFeO_3 + x$ wt%MnO_2 (BCT-67BF:Mn100x, $x = 0–0.6$) ceramics were systematically investigated, The structure–property relationship and possible mechanisms were discussed intensively.

2. Experimental procedures

The BCT-67BF:Mn100x ($x = 0–0.6$) ceramics were prepared by a conventional sintering method with the raw materials of $BaCO_3$ (99.0%), $CaCO_3$ (99.0%), TiO_2 (99.0%), Fe_2O_3 (99.99%) and MnO_2(98.0%). The powders were mixed according to the stoichiometric formula and ball-milled in alcohol for 24 h to get a homogeneous mixture. Each slurry was dried, and then calcined at 850 °C for 3 h. The calcined powders were ball milled again for 24 h, dried, and then pressed into disks of 13 mm in diameter and 0.6–1.0 mm in thickness under 80 MPa using 8 wt% polyvinyl alcohol (PVA) as binder, which was burnt out by slow heating at 550 °C for 2 h. Sintering was conducted between 1000 °C and 1040 °C in air for 1 h, lower sintering temperature for compositions with higher Mn content. The samples were embedded in the corresponding powder to reduce the evaporation of Bi during sintering. All the samples had relative densities higher than 94%.

The phase structure of the samples were characterized by X-ray powder diffraction (XRD, D/max 2400: Rigaku Inc. D, Japan) with Cu kα radiation. A scanning electron microscopy (SEM, Quanta 200 FEG System: FEI Co., USA) was used to determine grain size and microstructural uniformity of the samples. For measurements of electrical properties, both circular surfaces of the samples were painted with silver pastes and fired at 600 °C for 30 min. FE hysteresis loops and the polarization current intensity-electric field ($j-E$) loops were measured at RT at 10 Hz by precision premier II (Radiant Technology, Inc, Albuquerque, NM). Dielectric properties were measured upon heating from 30 °C to 480 °C at 1 kHz – 100 kHz using an Agilent E4980A precision LCR meter. For piezoelectric measurement, the samples were poled in silicone oil with applied electric field of 20 kV/cm–35 kV/cm for 20 min at 20 – 100 °C. The piezoelectric constant d_{33} was measured using a quasi-static d_{33} meter (ZJ-4A, Institute of Acoustics, Chinese Academy of Sciences, China). The planar electromechanical coupling factors k_p and the mechanical quality factor Q_m were measured by a resonance-antiresonance method using an impedance analyzer (Agilent 4294A) and calculated following IEEE standards. The magnetic properties of the powder samples were achieved at RT using a vibrating sample magnetometer (VSM, Lakeshore7300, USA). The relative dielectric constant with different magnetic field applied was measured using Agilent E4980A precision LCR meter at RT.

3. Results and discussion

Fig. 1(a) shows the XRD patterns of the BCT-67BF:Mn100x ($x = 0–0.6$) ceramics. All the ceramics show perovskite structures with no trace of impurity phases. Further detailed XRD analyses in the 2θ range from 38.5° to 46.5° are shown in Fig. 1(b). The tetragonal symmetry is characterized by the (002)/(200) splitting peaks at $2\theta \sim 45°$ and the existence of a single (111) peak at $2\theta \sim 40°$ [28], and pure rhombohedral BF has (003)/(021) peaks near $2\theta \sim 39.2°$ and (202) peak near $2\theta \sim 45.5°$ [29]. So the split (003)/(021) peaks near $2\theta \sim 39.2°$ and the distinct peak splitting near $2\theta \sim 45°$ corresponding to T(002)/T(200) and R(202) indicates that T and R phases coexisted in the ceramics with $x = 0–0.6$.

It is suggested that radii of Mn ions (Mn^{2+}: 0.67 Å, Mn^{3+}: 0.64 Å, and Mn^{4+}: 0.53 Å) are much smaller than that of A-site ions (Ba^{2+}: 1.35 Å, Ca^{2+}: 0.99 Å, and Bi^{2+}: 1.38 Å), and closer to that of B-site ions (Ti^{4+}: 0.68 Å, and Fe^{3+}: 0.645 Å). Mn ions might prefer to substitute for the B-site Ti^{4+} or Fe^{3+} to form a stable perovskite structure for their similar ionic radii. Moreover, according to reports, MnO_2 converts into Mn_2O_3, Mn_3O_4 at 650 °C and 980 °C in air respectively [22,30], and a change of valence state from Mn^{4+} to Mn^{3+} has been observed in Mn doped $(K_{0.5}Na_{0.5}Li_{0.065})NbO_3$

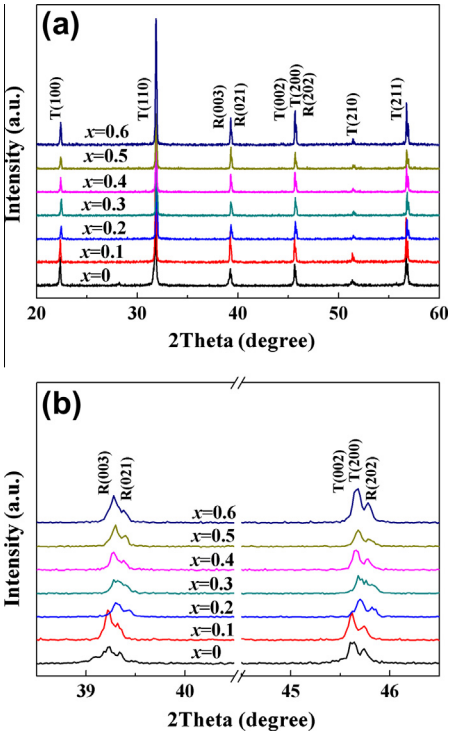

Fig. 1. (a) XRD patterns of the BCT-67BF:Mn100x ceramics with $x = 0–0.6$. (b) Expanded view of XRD patterns of the BCT-67BF:Mn100x ceramics.

ceramics using synchrotron X-ray absorption spectroscopy [31]. In our cases, all ceramics were sintered at 1000 °C –1040 °C in air, so it is possible that the Mn ions may have Mn^{3+} chemical states. In addition, the reaction between Mn^{3+} and Fe^{2+}: $Mn^{3+} + Fe^{2+} \rightarrow Mn^{2+} + Fe^{3+}$, effectively restrains the conversion of Fe^{3+} to Fe^{2+} and leads to the appearance of Mn^{2+} in the doped ceramics [22]. So Mn ions in our cases may have mixed valences of + 2, + 3, and + 4.

Fig. 2 shows the SEM microstructural images of the BCT-67BF:Mn100x (x = 0–0.6) ceramics. It can be seen that the undoped ceramic has large inhomogeneous grains and significant residual porosity, while the doped ceramics have elliptic grain morphologies with improved densification. This observation indicates that Mn doping significantly reduces the grain sizes and improves the sintering ability, which may be ascribed to the substitution of B-site ions by Mn cations, since Mn ions may occupy B site to form a stable perovskite structure and Mn ions can have + 2, + 3 and + 4 chemical states, and when Mn^{2+} ions substitute for Fe^{3+} or Mn^{3+} ions substitute for Ti^{4+}, oxygen vacancies will be created to compensate the charge imbalance [14,22,25], which results in slower ion motion, and consequently lower grain growth rate [17,32].

Figs. 3(a)–(g) shows the temperature-dependent relative dielectric constant (ε_r) of the BCT-67BF:Mn100x ceramics (x = 0–0.6) measured at different frequencies. All the ceramics show frequency-dependent, broadened dielectric permittivity peaks. The temperature corresponding to the maximum relative dielectric constant (T_m) is frequency-dependent and T_m shifts to higher temperature with increasing frequency, indicating their relaxor behaviors. To analyze the effects of Mn content on the relaxation characters of BCT-67BF ceramics, the modified Curie-Weis law is described as follows [33]:

$$\frac{1}{\varepsilon_r} - \frac{1}{\varepsilon_{rm}} = \frac{(T - T_m)^\gamma}{C} \quad (1)$$

where γ and C are constants and $1 \leqslant \gamma \leqslant 2$. The degree of relaxor behaviors could be estimated by the parameter γ. For normal ferroelectrics, γ = 1 and the ε_r above T_C obeys the Curie-Weis law. While for an ideal relaxor ferroelectric, γ = 2 and the ε_r deviates from the Curie-Weis law above T_m [33]. The $\ln(1/\varepsilon_r - 1/\varepsilon_{rm})$ versus $\ln(T - T_m)$ plots for all the ceramics are given in the insets of Figs. 3(a)–(g). The γ values determined from the corresponding slope of the fitting curves are 1.852, 1.910, 1.941, 1.976, 1.977, 1.978, and 1.980 for x = 0, 0.1, 0.2, 0.3, 0.4, 0.5, and 0.6 respectively. It can be seen that with increasing x, γ increases monotonically, indicating the enhanced relaxor behaviors, which are partially ascribed to the domain refinement and the weakening of long-range

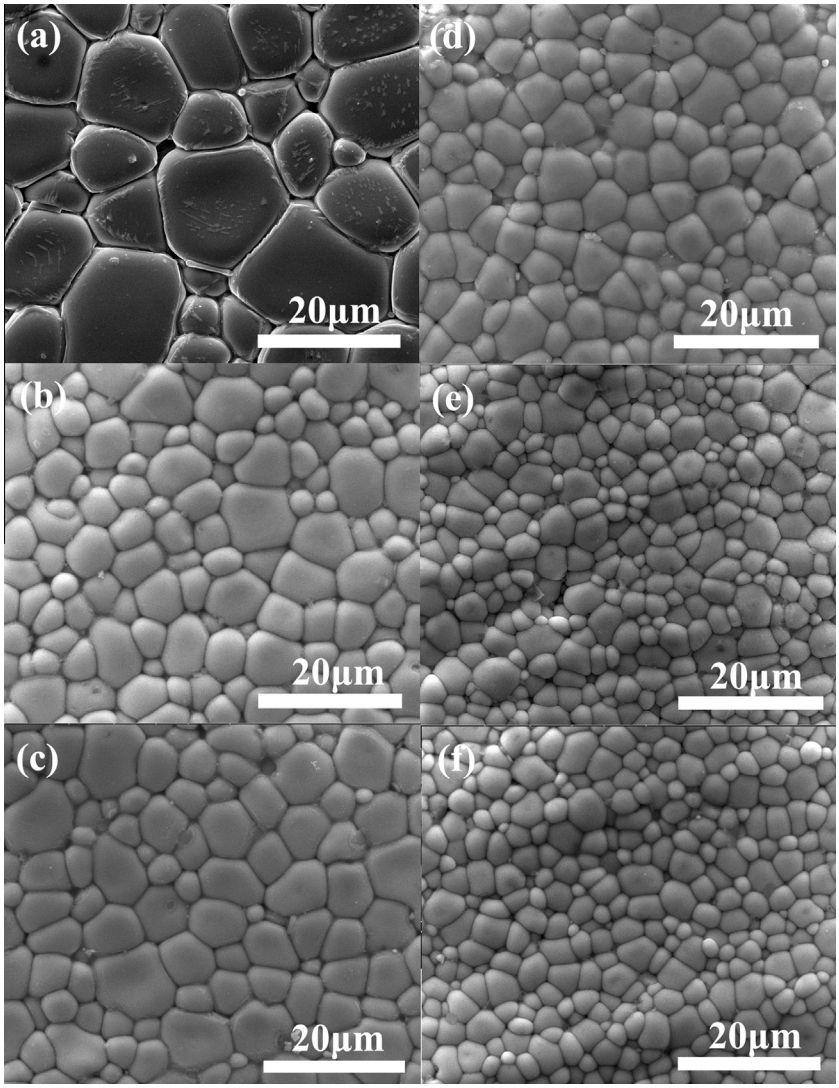

Fig. 2. SEM micrographs of the BCT-67BF:Mn100x ceramics (a) x = 0, (b) x = 0.1, (c) x = 0.2, (d) x = 0.4. (e) x = 0.5 and (f) x = 0.6.

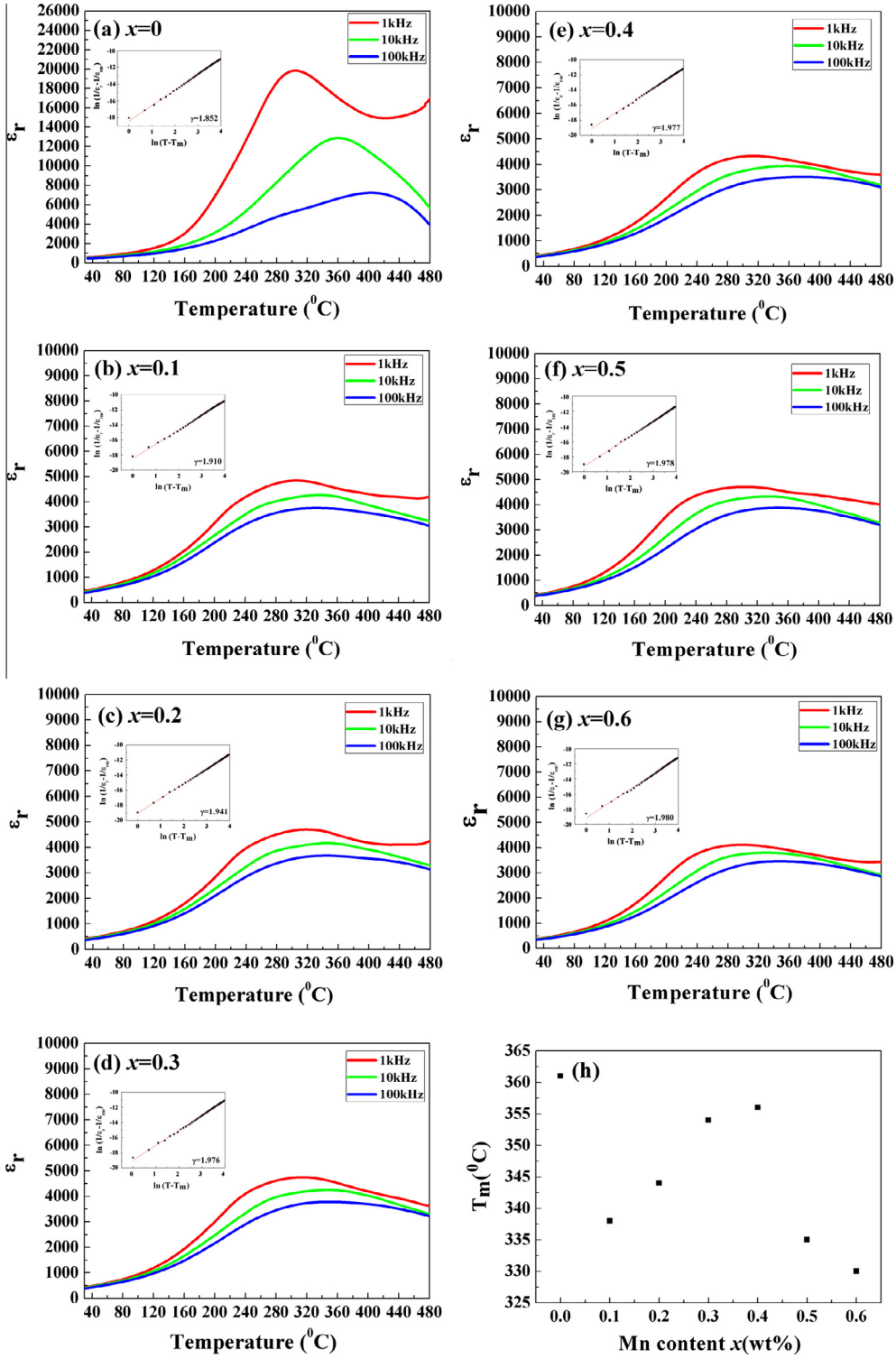

Fig. 3. Temperature-dependent dielectric properties of the BCT-67BF:Mn100*x* ceramics (a) $x = 0$, (b) $x = 0.1$, (c) $x = 0.2$, (d) $x = 0.3$, (e) $x = 0.4$, (f) $x = 0.5$, (g) $x = 0.6$ (Insets are the corresponding curves of $\ln(1/\varepsilon_r - 1/\varepsilon_{rm})$ against $\ln(T - T_m)$ at 10 kHz), (h) T_m of the BCT-67BF:Mn100*x* ceramics as a function of Mn content at 10 kHz.

ferroelectric interactions caused by Mn doping [34]. In BCT-67BF:Mn100*x* ceramics, the appearance of oxygen vacancies for charge compensation caused by B-sites Mn doping may disrupt the long-range ferroelectric ordering [22,25], resulting in enhanced relaxor behavior. Additionally, it is known that fine-grained BT-based ceramics show higher inner stress due to 90° domain walls, and the inner stress increases with the grain size decreases [35]. Higher inner stress can also promote the appearance of typical relaxor behavior [36].

The T_m versus Mn content curves of the BCT-67BF:Mn *x* ceramics measured at 10 kHz are plotted in Fig. 3(h). Obviously, the T_m of all the doped ceramics are lower than that of undoped counterparts, this observation is similar to that of Mn doped 0.7BF-0.3BT solid solutions [22]. It is generally suggested that the

intensity of Mn–O bond is lower than that of Ti–O bond [22], the substitution of Ti or Fe ions by Mn ions will weaken the ferroelectric state of BCT-67BF:Mn x ceramics, resulting in decreased T_m. However, in our cases, it is observed that with increasing Mn doping, T_m increases slowly, reaching the maximum of 356 °C near $x = 0.4$, then decreases to 330 °C at $x = 0.6$. The phase transitions of the doped ceramics may be related to the cell volume effect induced by the grain size [35] and the interior bias electric field caused by Mn doping. The exact origin of the change of T_m in the ceramics is still unclear and left for further studies.

Figs. 4(a)–(g) shows the RT polarization–electric field (P–E) hysteresis loops of the BCT-67BF:Mn100x ($x = 0$–0.6) ceramics measured with the applied field of 70 kV/cm. The undoped ceramics possesses a typical ferroelectric hysteresis loop with a saturation tendency, while the loops of the Mn-doped ceramics are very slim, consistent with the appearance of typical ferroelectric relaxor behaviors [34]. Fig. 4(h) plots the variation of maximum polarization (P_{max}), remnant polarization (P_r) and coercive field (E_C) of the BCT-67BF:Mn100x ceramics against Mn content. It can be seen that with increasing Mn doping, P_{max}, P_r, and E_C decrease simultaneously, indicating the weakened ferroelectricity.

The most important evidence of ferroelectricity is P–E hysteresis loop. However, there exists a certain insulation leakage in actual ferroelectrics, which makes the measured P–E loops deviate from

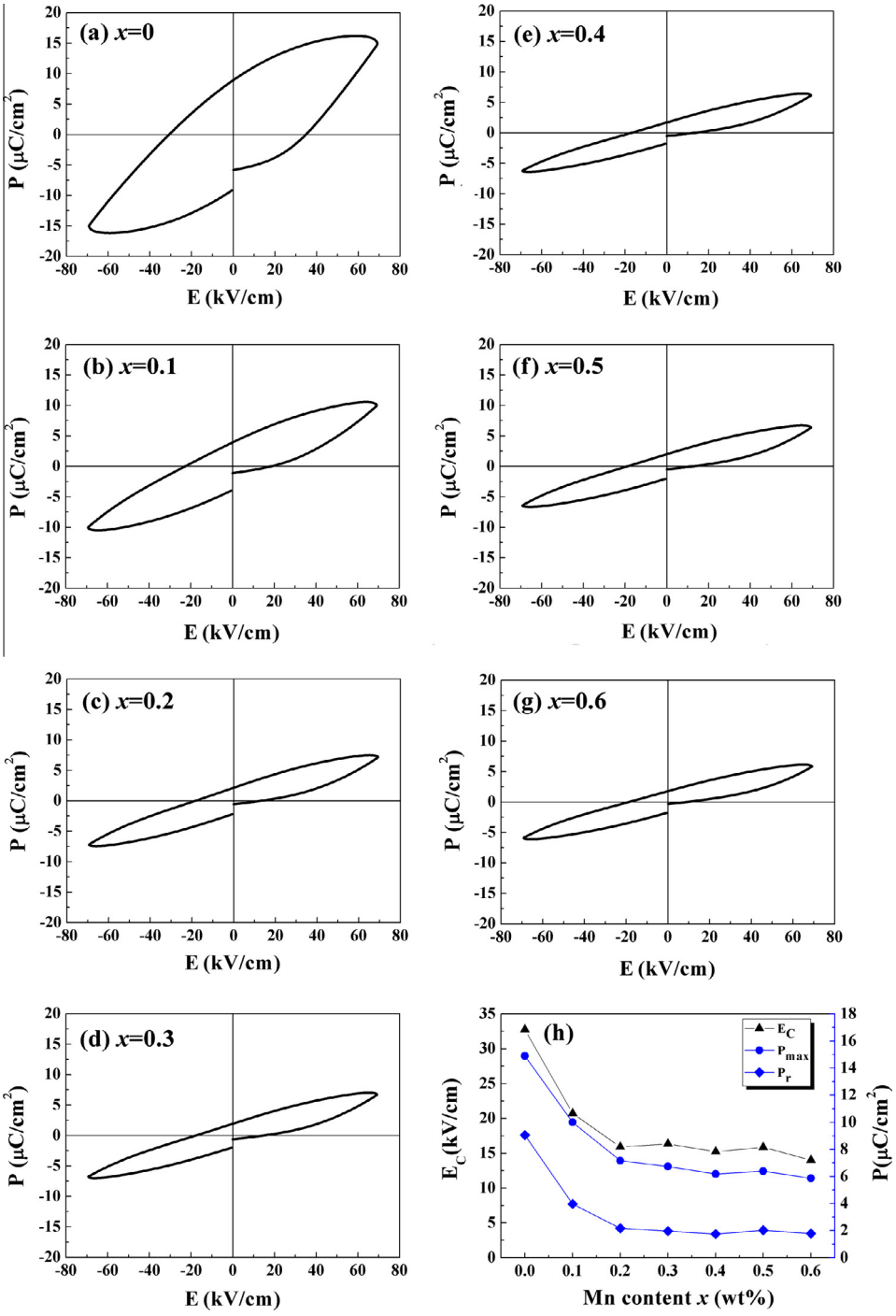

Fig. 4. Room temperature P-E hysteresis loops of the BCT-67BF:Mn100x ceramics measured at 10 Hz (a) $x = 0$, (b) $x = 0.1$, (c) $x = 0.2$, (d) $x = 0.3$, (e) $x = 0.4$, (f) $x = 0.5$, (g) $x = 0.6$ and (h) P_{max}, P_r and E_C values of the BCT-67BF:Mn100x ceramics as a function of Mn content.

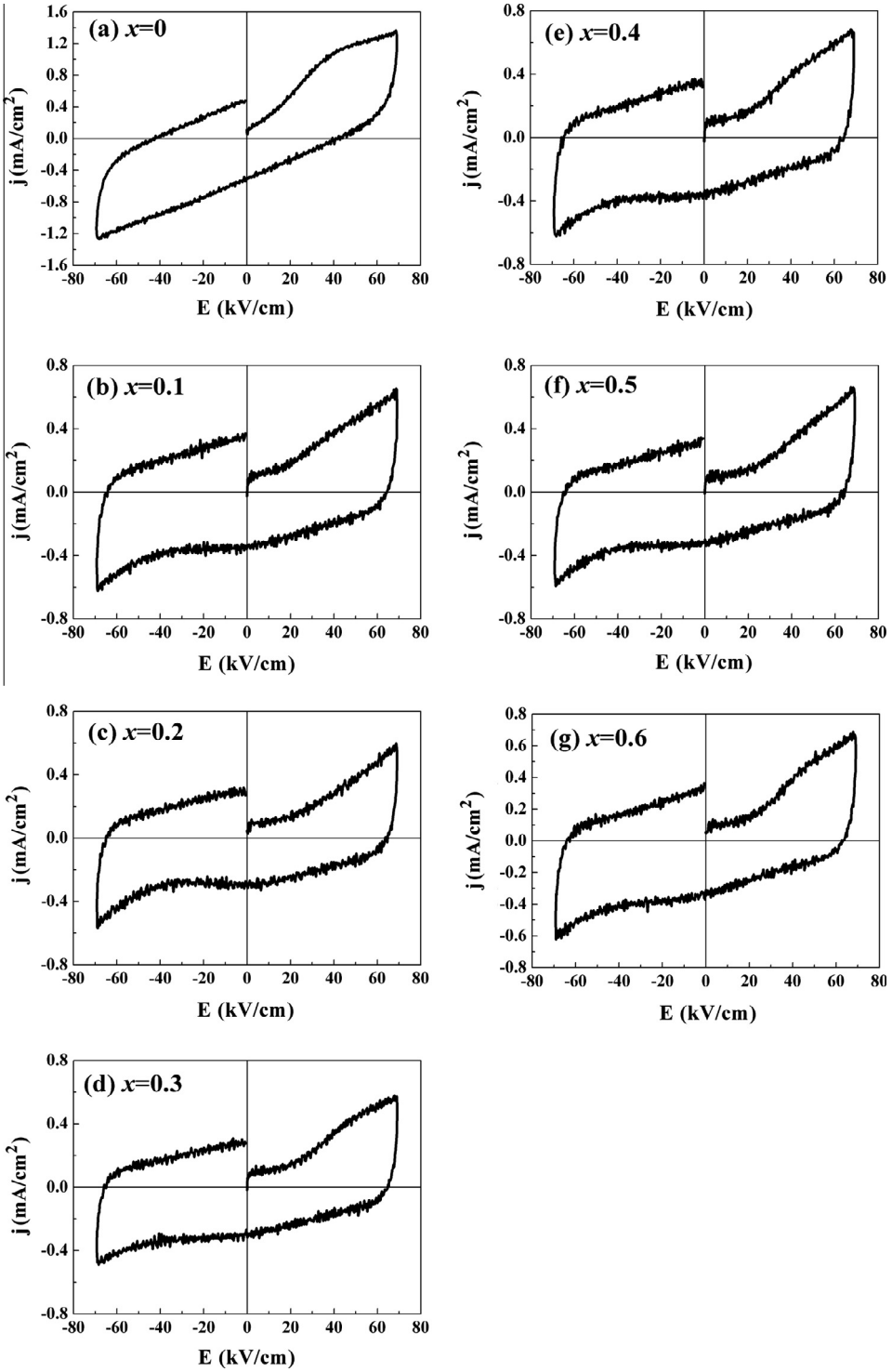

Fig. 5. Room temperature polarization current intensity–electric field loops of the BCT-67BF:Mn100*x* ceramics measured at 10 Hz (a) $x = 0.0$, (b) $x = 0.1$, (c) $x = 0.2$, (d) $x = 0.3$, (e) $x = 0.4$, (f) $x = 0.5$ and (g) $x = 0.6$.

actual ones [37]. The *P*–*E* loops of the ceramics are dominated by the contributions of leakage currents, domain switching and linear capacitance. Furthermore, the hysteresis-like "loop" may also occur in non-ferroelectric systems [37–39]. It has been reported that some lossy dielectrics exhibit cigar-shaped *P*–*E* "loop" which have little to do with ferroelectricity [39]. The reorientation of polarization could not be easily detected from *P*–*E* loops. It is suggested that distinguishing the contributions of linear capacitance, electric conductivity and domain switching in current-electric field loops is an effective way to observe the reorientation of polarization and measure ferroelectricity of the materials studied [37,40]. Figs. 5(a)–(g) shows the polarization current intensity–electric filed (*j*–*E*) curves of BCT-67BF:Mn100*x* ceramics ($x = 0$–0.6) measured with the applied field of 70 kV/cm. The polarization current intensity of all ceramics show very broad and flat peaks at the nonergodic state, indicating ferroelectric domains reversal

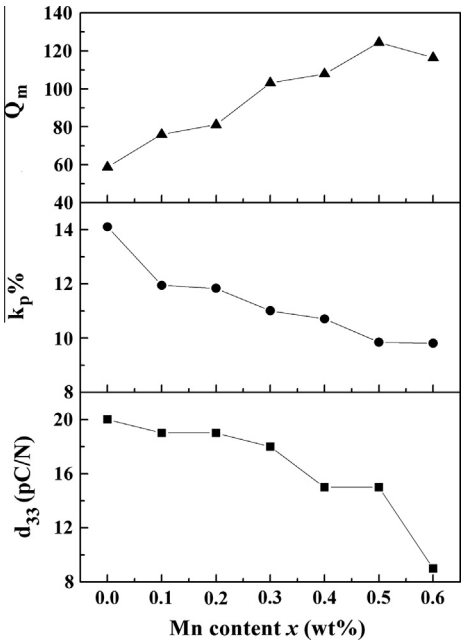

Fig. 6. d_{33}, k_p, and Q_m values of the BCT-67BF:Mn100x ceramics as a function of Mn content.

and relaxor behaviors [37]. A small amount of Mn doping effectively decreases the leakage current of BCT-67BF ceramics, indicating the enhanced resistivity. The large leakage current in undoped ceramics may be ascribed to the mix valance of Fe ions and oxygen vacancies. The reaction between Mn^{3+} and Fe^{2+}: $Mn^{3+} + Fe^{2+} \rightarrow Mn^{2+} + Fe^{3+}$, effectively restrains the conversion of Fe^{3+} to Fe^{2+}, increases the resistivity of the Mn doped ceramics [22].

The undoped ceramics show the optimal ferroelectric property with $P_r = 9.1\ \mu C/cm^2$, which may be induced by the larger leakage current and domain switching as shown in Fig. 5(a) [37,40] The weakened ferroelectric properties in Mn doped ceramics may be ascribed to the pinning effect on domain reversal caused by the increased oxygen vacancies with increasing Mn doping [22], which are detrimental for FE property and the observation of saturated polarization. On the other hand, the significantly decreased grain size caused by Mn doping (as shown in Fig. 2) is an extrinsic effect for the weakened ferroelectricity. Small grain size means large amount of grain boundary, which leads to polarization discontinuity between grains and hence decreased polarization [41]. The effect of grain size on the ferroelectricity of the BCT-67BF:Mn100x ceramics can be interpreted with the theory of P–E hysteresis loop based on the Avrami model proposed by *Orihara* [42]. For ferroelectrics, the proportion of grains' contribution in polarization reverse (f) can be expressed as follows:

$$f = f_0[1 - \exp(-G_a d^3/kT)] \quad (2)$$

where G_a is a constant representing the grain anisotropy energy density, k is the Boltzmann constant and d is the grain size [35,42]. From this equation, f has relevance only with the grain size d. Therefore, the proportion of grains' contribution in polarization reverses decreases with decreasing the grain size, resulting in the weakened ferroelectric properties.

The variations of RT piezoelectric constant (d_{33}), planar electromechanical coupling factor (k_p), and mechanical quality factor (Q_m) against Mn content are shown in Fig. 6. It can be seen that d_{33} and k_p decrease simultaneously with increasing Mn doping, consistent with the variation of ferroelectricity with Mn content. The weakened piezoelectricity caused by Mn doping may be explained using the thermodynamic theory of ferroelectrics proposed by *Haun* et al. [43] P_r is proportional to d_{33}, which can be expressed as follows:

$$d_{33} = 2Q_{11}P_r\varepsilon_{33} \quad (3)$$

where Q_{11} is the electrostrictive coefficient which is a constant for perovskite materials, ε_{33} is the dielectric constant. And the relationship between k_p and P_r can be expressed as follows [35,44]:

$$k_p = 2\left[\frac{2\varepsilon_{33}^T}{(1-\sigma)S_{11}^E g_{31}}\right]^{1/2} P_r \quad (4)$$

where ϵ_{33}^T is the free dielectric constant, S_{11}^E is the elastic compliance constant measured at short circuit, σ is Poisson ratio, g_{31} is the piezoelectric constant. The relationship between the piezoelectric property and FE property indicates that the weakened ferroelectricity may be responsible for the weakened piezoelectricity. Whereas, Q_m increases with increasing x and reaches the maximum of 124 at $x = 0.5$, and then slightly decreases.

The RT magnetization-magnetic field (M–H) hysteresis loops of the BCT-67BF:Mn100x (x = 0–0.6) ceramics were measured with a maximum magnetic field of 10 kOe, as shown in Figs. 7(a)–(g). The hysteresis loops indicates the ferromagnetic nature of the BCT-67BF:Mn100x ceramics (x = 0–0.6) at RT. It has been suggested that the spatially modulated spiral spin structure of BF can be suppressed by doping [9,45], actually, doping can even lead to a transition from the spinodal structure of pure BF to the homogeneous FM state [46]. Hence the origin of the net magnetization of the BCT-67BF:Mn100x ceramics can be ascribed to three possible aspects: Firstly, the bond angle of Fe–O–Fe may be changed and the spiral spin structure might be suppressed or even destructed by Mn doping. Secondly, according to Goodenough - Kanamori rules [47], a FM interaction should appear between the e_g electrons of the $Fe^{3+}(d^5)$ and the t_{2g} electrons of the $Mn^{4+}(d^3)$ [25]. And thirdly, as mentioned above, Fe^{2+} or oxygen vacancies may appear to compensate the charge imbalance arising from the co-substitution of Bi^{3+} by Ba^{2+}, Ca^{2+} ions, Fe^{3+} by Ti^{4+}, Mn ions. If Fe^{2+} exists, the statistical distribution of Fe^{3+} and Fe^{2+} ions in octahedral spaces may also lead to net magnetization and ferromagnetism [14,19].

The variation of the maximum magnetization (M_{max}), remnant magnetization (M_r) and coercive field (H_C) with the Mn content is present in Fig. 7(h). M_{max}, M_r and H_C increase with increasing x simultaneously, reach the maximum values of 0.78 emu/g, 0.34 emu/g, and 2.67 kOe respectively at $x = 0.5$, which indicates that the FM properties of BCT-67BF ceramics could be improved by appropriate Mn doping. According to the Jahn–Teller effect [22], Mn^{3+} ions substitute for Fe^{3+} or Ti^{4+} and enter into oxygen octahedron, the lattice around the Mn^{3+} ions may distort, reducing the symmetry of the crystal [22]. So, the M_{max} and M_r increase with increasing Mn doping till $x = 0.5$, similar to the variation of magnetism with Mn content in Mn doped 0.7BF-0.3BT solid solution [22]. However, with further increasing Mn content, based on Goodenough - Kanamori rules [47], the FM interaction between the e_g electrons of the $Fe^{3+}(d^5)$ ions and the t_{2g} electrons of the $Mn^{4+}(d^3)$ ions can be slightly decreased by the conversion of MnO_2 into Mn_2O_3, Mn_3O_4 at 650 °C, 980 °C [30] and the reaction between Mn^{3+} and Fe^{2+}: $Mn^{3+} + Fe^{2+} \rightarrow Mn^{2+} + Fe^{3+}$. Additionally, the high coercive magnetic field may be related to the pinning effect of magnetic domain walls and the magnetic anisotropy [29].

Frequency dependence of the RT relative dielectric constant (ε_r) for the BCT-67BF:Mn100x ceramics were firstly measured without magnetic field, as shown in Fig. 8(a). It is evident that the ε_r values of all the samples are frequency dependent, decrease first, and then gradually become nearly constant at high frequencies (about 200 kHz). For the compositions with x = 0, 0.1, 0.2, 0.3, 0.4, 0.5 and 0.6, the RT ε_r at 1 kHz are 498, 488, 457, 398, 382, 374, and

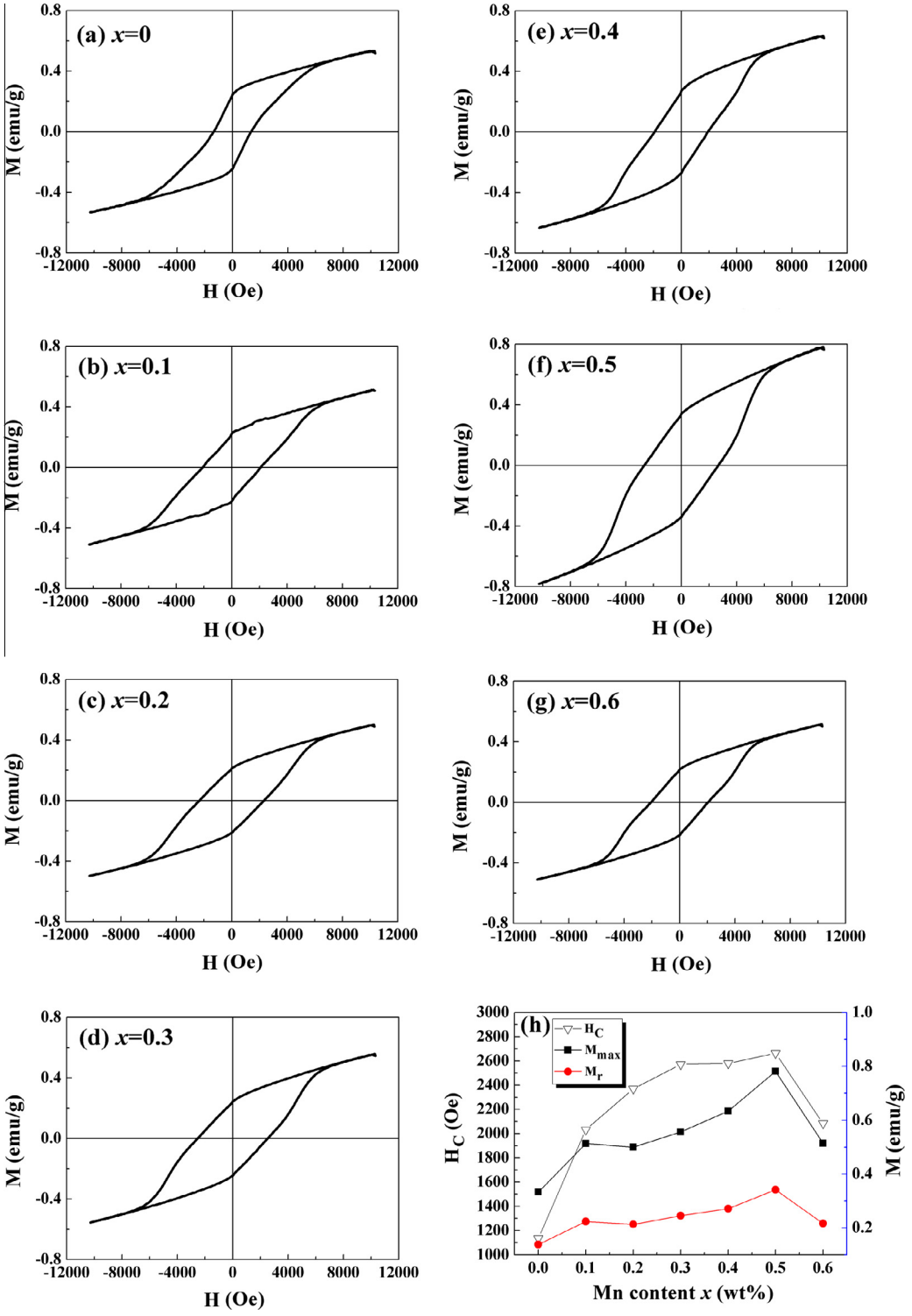

Fig. 7. Room temperature magnetic hysteresis loops of the BCT-67BF:Mn100*x* ceramics (a) $x = 0$, (b) $x = 0.1$, (c) $x = 0.2$, (d) $x = 0.3$, (e) $x = 0.4$, (f) $x = 0.5$, (g) $x = 0.6$ and (h) M_{max}, M_r and H_C values of the BCT-67BF:Mn100*x* ceramics as a function of Mn content.

360 respectively, and the dielectric loss at 1 kHz are 0.16, 0.04, 0.03, 0.03, 0.03, 0.03 and 0.02 respectively. As can be seen, the introduction of Mn significantly decreases the RT ε_r and dielectric loss.

The coexistence of FE and FM properties is achieved in the BCT-67BF:Mn100*x* ceramics, so coupling between them could be expected. To investigate the coupling between electric and magnetic orders, the variation of the RT ε_r with a gradually increasing applied magnetic field is measured at 200 kHz, as shown in Fig. 8(b). The magnetocapacitive coefficient, defined as the relative change of the dielectric constant as a function of the applied magnetic filed and expressed as $((\varepsilon_r(H)-\varepsilon_r(0))/\varepsilon_r(0))$, is commonly used to describe the magnetocapacitive effect of multiferroics [6,25,29]. From Fig. 8(b), it is clear that with increasing applied magnetic field, the RT ε_r increases and the positive values of magneto-capacitance depend on the doping concentration of

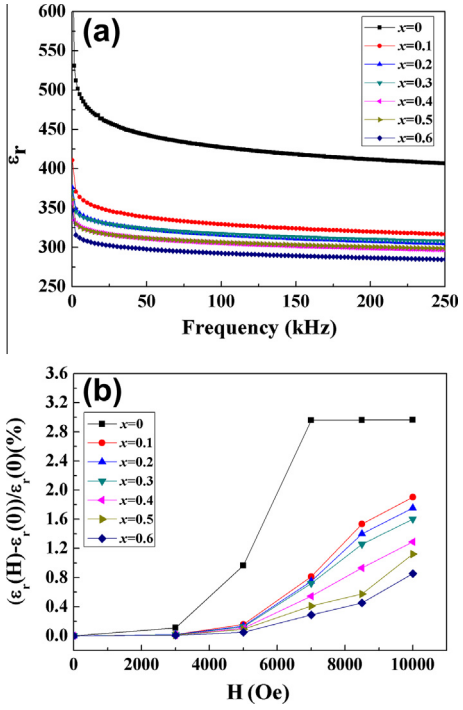

Fig. 8. (a) Frequency-dependent ε_r of the BCT-67BF:Mn100x ceramics with x = 0–0.6. (b) Magnetic field - induced change in the room temperature ε_r of the BCT-67BF:Mn100x ceramics with x = 0–0.6.

Mn. At RT with ΔH = 10 kOe, the magnetocapacitive coefficient values are 2.96%, 1.90%, 1.76%, 1.60%, 1.29%, 1.12%, and 0.86% for the compositions with x = 0, 0.1, 0.2, 0.3, 0.4, 0.5, and 0.6 respectively, These values possess the same magnitude order with that reported in Ref. [14]. The observed large magneto-capacitance indicates that strong coupling exists between the FE and FM orders in the BCT-67BF:Mn100x ceramics and Mn doped BCT-67BF ceramics have potential applications in multiple state memory devices, spintronics, transducer, electric field controlled ferromagnetic resonance devices and magneto-electric sensor devices, etc. The magnetocapacitive effect of the BCT-67BF:Mn100x ceramics could be interpreted as follows. The multiferroics will be strained when a magnetic field is applied. The coupling between the magnetic and FE domains will make the strain to induce a stress and then generate an electric field. This field could orient the FE domains, leading to modification of the dielectric behavior [25,48]. The decreased magnetocapacitive effect with increasing Mn content may attribute to the decreased ferroelectricity.

4. Conclusions

In summary, the structures, electric, magnetic, and magnetocapacitive properties of the BCT-67BF:Mn100x (x = 0–0.6) ceramics were intensively investigated. The ceramics have diphasic T and R phases when $x \leqslant 0.6$. An increase of Mn doping improves the densification, enhances the relaxor behavior and significantly decreases the grain size. The room temperature relative dielectric constant and dielectric loss decrease simultaneously with increasing x. With increasing Mn doping, the ferroelectricity and piezoelectricity weaken monotonically, while the ferromagnetism enhances significantly, reaches the maximum near x = 0.5, and then weakens. Additionally, the magnetocapacitive coefficient $(\varepsilon_r(H) - \varepsilon_r(0))/\varepsilon_r(0)$ decreases with increasing x.

Acknowledgements

This work was supported by the National Science and Technology Support Program (SQ2012BAJY3766), the National Key Basic Research Program of China (973 Program, 2013CB632900), the National Nature Science Foundation of China (10704021, 51102062, and 11174127), the Key Scientific and Technological Project of Harbin (Grant No. 2009AA3BS131).

References

[1] M. Kumar, S. Shankar, R.K. Kotnala, O. Parkash, J. Alloys Comp. 577 (2013) 222–227.
[2] W. Eerenstein, N.D. Mathur, J.F. Scott, Nature (London). 442 (2006) 759–765.
[3] N.A. Spaldin, M. Fiebig, Science. 309 (2005) 391–392.
[4] J. Ma, J.M. Hu, Z. Li, C.W. Nan, Adv. Mater. 23 (2011) 1062–1087.
[5] D.P. Dutta, B.P. Mandal, R. Naik, G. Lawes, A.K. Tyagi, J. Phy, J. Phys. Chem. C. 117 (2013) 2382–2389.
[6] P.K. Patel, K.L. Yadav, Mater. Res. Bull. 48 (2013) 1435–1438.
[7] X.Y. Mao, H. Sun, W. Wang, X.B. Chen, Appl. Phys. Lett. 102 (2013) 072904.
[8] S.C. Yang, A. Kumar, V. Petkov, S. Priya, J. Appl. Phys. 113 (2013) 114101.
[9] H.L. Deng, M. Zhang, Z. Hu, Q.F. Xie, Q. Zhong, J.Z. Wei, H. Yan, J. Alloys Comp. 582 (2014) 273–276.
[10] W.W. Mao, X.F. Wang, Y.M. Han, X.A. Li, Y.T. Li, Y.F. Wang, Y.W. Ma, X.M. Feng, T. Yang, J.P. Yang, W. Huang, J. Alloys Comp. 584 (2014) 520–523.
[11] W.W. Mao, X.A. Li, Y.T. Li, X.W. Wang, Y.F. Wang, Y.W. Ma, X.M. Feng, T. Yang, J.P. Yang, Mater. Lett. 97 (2013) 56–58.
[12] S. Chauhan, M. Arora, P.C. Sati, S. Chhoker, S.C. Katyal, M. Kumar, Ceram. Int. 39 (2013) 6399–6405.
[13] G.F. Cheng, Y.J. Ruan, Y.H. Huang, X.S. Wu, J. Alloys Comp. 566 (2013) 235–238.
[14] A. Ianculescua, F.P. Gheorghiub, P. Postolacheb, O. Opreaa, L. Mitoseriub, J. Alloys Comp. 504 (2010) 420–426.
[15] X. Xue, G.Q. Tan, J. Alloys Comp. 575 (2013) 90–95.
[16] S.N. Tripathy, B.G. Mishra, M.M. Shirolkar, S. Sen, S.R. Das, D.B. Janes, D.K. Pradhan, Mater. Chem. Phys. 141 (2013) 423–431.
[17] Z.M. Tian, Y.S. Zhang, S.L. Yuan, M.S. Wu, C.H. Wang, Z.Z. Ma, S.X. Huo, H.N. Duan, Mater .Scien. Engin .B. 177 (2012) 74–78.
[18] H. Singh, A. Kumar, K.L. Yadav, Mater. Sci. Eng. B. 176 (2011) 540–547.
[19] F.P. Gheorghiua, A. Ianculescub, P. Postolachea, N. Lupuc, M. Dobromira, D. Lucaa, L. Mitoseriua, J. Alloys Comp. 506 (2010) 862–867.
[20] J.L. Xu, D. Xie, C. Yin, T.T. Feng, J. Appl. Phys. 114 (2013) 154103.
[21] M. Kubota, K. Oka, H. Yabuta, K. Miura, M. Azuma, Inorg. Chem. 52 (2013) 10698–10704.
[22] X.H. Liu, Z. Xu, S.B. Qu, X.Y. Wei, J.L. Chen, Ceram. Int. 34 (2008) 797–801.
[23] X.K. Wei, Y.T. Su, Y. Sui, Z.X. Zhou, Y. Yao, C.Q. Jin, R. C Yu, Appl. Phys. Lett. 102 (2013) 242910.
[24] H.B. Yang, C.R. Zhou, X.Y. Liu, Q. Zhou, G.H. Chen, W.Z. Li, H. Wang, J. Eur. Ceram. Soc. 33 (2013) 1177–1183.
[25] L.H. Yin, W.H. Song, X.L. Jiao, W.B. Wu, X.B. Zhu, Z.R. Yang, J.M. Dai, R.L. Zhang, Y.P. Sun, J. Phys. D: Appl. Phys. 42 (2009) 205402.
[26] L.F. Zhu, B.P. Zhang, X.K. Zhao, L. Zhao, P.F. Zhou, J.F. Li, J. Am. Ceram. Soc. 96 (2013) 241–245.
[27] X.S. Wang, H. Yamada, C.N. Xu, Appl. Phys. Lett. 86 (2005) 022905.
[28] A. Ullah, C.W. Ahn, S.Y. Lee, J.S. Kim, I.W. Kim, Ceram. Int. 38 (2012) 363–368.
[29] D.H. Wang, W.C. Goh, M. Ning, C.K. Ong, Appl. Phys. Lett. 88 (2006) 212907.
[30] F.M. Zhang, Piezoelect. Acoustoopt. 20 (1998) 358–360.
[31] S. Wongsaenmai, K. Kanchiang, S. Chandarak, Y. Laosiritaworn, S. Rujirawat, R. Yimnirum, Curr. Appl. Phys. 12 (2012) 418–421.
[32] M. Kumar, K.L. Yadav, Appl. Phys. Lett. 91 (2007) 112911.
[33] K. Uchino, S. Nomura, Ferroelectr. Lett. Sect. 44 (1982) 55–61.
[34] Q. Tan, D. Viehland, Ferroelectrics. 193 (1997) 157–165.
[35] J.G. Hao, W.F. Bai, W. Li, J.W. Zhai, J. Am. Ceram. Soc. 95 (2012) 1998–2006.
[36] H. Yu, H.X. Liu, H. Hao, L.L. Guo, C.J. Jin, Z.Y. Yu, M.H. Cao, Appl. Phys. Lett. 91 (2007) 222911.
[37] L. Wang, X.L. Wang, J. Shi, Ferroelectrics 411 (2011) 86–92.
[38] A. Loidl, S. Krohns, J. Hemberger, P. Lunkenheimer, J. Phys.: Condens. Matter 20 (2008) 191001–191003.
[39] J.F. Scott, J. Phys, Condens. Matter. 20 (2008) 021001–021002.
[40] H. Yan, F. Inam, G. Viola, H. Ning, H. Zhang, Q. Jiang, T. Zeng, Z. Gao, M.J. Reece, J. Adv. Dielectr. 1 (2011) 107–118.
[41] P.A. Jha, A.K. Jha, J. Alloys Comp. 513 (2012) 580–585.
[42] H. Orihara, S. Hashimoto, Y. Ishibashi, J. Phys. Soc. Jpn. 63 (1994) 1031–1035.
[43] M.J. Haun, E. Furman, S.J. Jang, L.E. Cross, Ferroelectrics. 99 (1989) 13–25.
[44] T. Yamamoto, Am. Ceram. Soc. Bull. 71 (1992) 978–985.
[45] V.A. Khomchenko, V.V. Shvartsman, P. Borisov, W. Kleemann, D.A. Kiselev, I.K. Bdikin, J.M. Vieira, A.L. Kholkin, J. Phys. D: Appl. Phys. 42 (2009) 045418.
[46] V.A. Khomchenko, D.A. Kiselev, J.M. Vieira, L. Jian, A.L. Kholkin, A.M.L. Lopes, Y.G. Pogorelov, J.P. Araujo, M. Maglione, J. Appl. Phys. 103 (2008) 024105.
[47] J.B. Goodenough, Phys. Rev. 100 (1955) 564–573.
[48] V.R. Palkar, D.C. Kundaliya, S.K. Malik, S. Bhattacharya, Phys. Rev. B 69 (2004) 212102.